Journal of Materials Chemistry B

ROYAL SOCIETY OF CHEMISTRY

PAPER

View Article Online
View Journal | View Issue

Cite this: J. Mater. Chem. B, 2024, 12, 8376

An excimer process induced a turn-on fluorescent probe for detection of ultra-low concentration of mercury ions†

Shujing Fang,[a] K. M. K. Swamy,[b] Wen-Yan Zan,[c] Juyoung Yoon*[b] and Shudi Liu*[a]

The accumulation of mercury pollution in plants can induce severe injury to human beings. It is a great challenge to monitor ultra-low concentrations of mercury in complicated matrixes. In this study, we successfully developed a strategy *via* Hg^{2+}-triggered naphthalene-based fluorescent **probe 1**, which formed excimer that subsequently emitted fluorescence for the successful detection of ultra-low concentrations of Hg^{2+}. The coordination of N and S atoms with Hg^{2+} facilitated the formation of excimer from the naphthalene-conjugated planes that were in sufficiently close proximity. Suppression of C=N bond rotation also induced the chelation-enhanced fluorescence (CHEF) effect, and the cumulative result of these effects was obvious fluorescent enhancement. Compared with **probe 2**, the other key factor for detection of Hg^{2+} is that the electrons of the hydroxyl group can easily transfer to a naphthalene moiety, resulting in an augmented π-electron density that enhanced the π–π stacking of the naphthalene-conjugated excimer. After detailed spectral studies and mechanism discussions, it was realized that **probe 1** was able to detect ultra-low concentrations of Hg^{2+} in PBS buffer solution. The detection limit was calculated to be 1.98 nM. On account of the excellent performances, the probe was successfully applied in monitoring Hg^{2+} in water and pea sprouts with the potential for application as an advanced warning of contamination.

Received 30th April 2024,
Accepted 20th July 2024

DOI: 10.1039/d4tb00934g

rsc.li/materials-b

Introduction

Mercury is widely distributed in the natural environment and exists in various forms. Volcanic eruptions, seismic activity, geological exploitation, gold mining, and oil refining are always accompanied by mercury contamination. The average mercury concentration was calculated to be more than 100 mg kg^{-1} in industrial and mining areas, which is higher than the background value of 0.4 mg kg^{-1}.[1] Potential leakage risks also originate from a variety of supplies used on a daily basis, ranging from preservatives in vaccines, dental consumables, thermometers, and high-pressure mercury lamps.[2,3] Mercury exposure is prevalent in daily life through inhaled air, drinking water, and food. Mercury does not degrade, and because it continuously accumulates in biological systems, the potential risk for contamination appears to be very serious and deserves adequate attention.[4,5]

Quantitative and qualitative measurements are necessary to accurately assess mercury pollution.[6,7] Efficient methods for mercury detection should be highly sensitive and selective to distinguish mercury from complicated matrixes. Commonly used methods are colorimetric analysis, atomic absorption spectrometry, and gas chromatography–mass spectrometry.[8] However, these methods require sophisticated procedures and expensive instruments, and they are not suitable for real-time *in situ* visual detection. In this respect, fluorescent probes have become powerful monitoring tools due to their excellent properties, such as small size, easy modification, high selectivity and sensitivity, perfect solubility and biocompatibility, non-invasiveness, and real-time *in situ* detection with high spatial and temporal resolution.[9–14]

Hundreds of fluorescent probes have been designed and used for Hg^{2+} monitoring based on diverse detection mechanisms.[15–22] However, excimer formation-induced fluorescent changes for Hg^{2+} are rare. Intramolecular or intermolecular excimers are mainly constructed with increased π–π electron stacking by fixing two or more planar chromophores at close distances. Besides, excimers can form in concentrated solutions

[a] College of Chemistry and Chemical Engineering, Yantai University, Yantai 264005, P. R. China. E-mail: liushd2018@163.com
[b] Department of Chemistry and Nanoscience, Ewha Womans University, Seoul, 03760, Korea. E-mail: jyoon@ewha.ac.kr
[c] Institute of Molecular Science, Shanxi University, Taiyuan, 030006, P. R. China

† Electronic supplementary information (ESI) available. See DOI: https://doi.org/10.1039/d4tb00934g

that induce the interaction of neighboring molecules.[23,24] Excimer-based fluorescent probes can provide built-in self-calibration for signal correction according to modulated monomer and excimer emission.[25–27]

The conformations of polycyclic aromatic hydrocarbons such as naphthalene, anthracene, naphthalimide, perylene, pyrene, and analogous derivatives are easily modulated with varying optical properties,[28–38] although certain disadvantages such as the solubility and short emission wavelength more or less limit their biological application.[39,40] In addition, sensitive detection of Hg^{2+} directly in aqueous solutions is difficult due to the pronounced hydration effects of Hg^{2+}. Amongst these aromatic fluorophores, naphthalene provides an excellent platform for functionalized design of fluorescent probes that will recognize specific substrates.[41–44] Facile modification of hydrophilic groups is essential to increase water solubility. Because of obvious advantages such as stable optical properties and selectivity, it is feasible for widespread development in different domains.

In this study, two fluorescent probes (1 and 2) were successfully synthesized by modifying mercaptoethylamine on a naphthalene fluorophore. The thiol and Schiff base moieties in **probe 1** drive the affinity coordination between S, N, and Hg^{2+}, triggering the fluorophores to be situated in sufficiently close proximity to yield excimer. The C=N group acting as a molecular rotor was restricted, and the inhibited isomerization mechanism induced turn-on fluorescence in the presence of Hg^{2+}.[45,46] Lone pairs of electrons of hydroxyl groups transferred to the naphthalene moiety, which also resulted in an augmented π-electron density that triggered π–π electron stacking. These interactions further tuned the emissions from monomer to excimer simultaneously, with obvious fluorescence enhancement.

Combining the solubility advantages of hydroxyl and thiol groups, this probe exhibited turn-on emission in the presence of ultra-low concentrations of Hg^{2+} in PBS buffer solution. The spectral spectroscopies were investigated involving sensitivity and selectivity testing, and the detection mechanism was identified by mass spectra. **probe 1** was finally applied for monitoring real water samples and imaging the roots of pea sprouts.

Results and discussion

Spectral studies of probe 1

probe 1 and **probe 2** were synthesized using the following procedures (Scheme 1) and were fully characterized by NMR and MS spectra, which appears in the ESI† (Fig. S1–S6). Having obtained **probe 1**, fluorescence spectral studies were performed for Hg^{2+} monitoring in different solutions. The fluorescence emission remained stable in organic solvents, including DMF, DMSO, THF, CH_2Cl_2, C_2H_5OH, and CH_3OH (Fig. S7, ESI†), while a slight fluctuation was exhibited in PBS buffer solution (Fig. 1). The phenomenon was ascribed to the self-assembly process of **probe 1** in PBS buffer to form an excimer with the assistance of hydrogen bonds of sulfydryl and hydroxyl groups, which was suggested by mass spectrum (Fig. S3, ESI†).

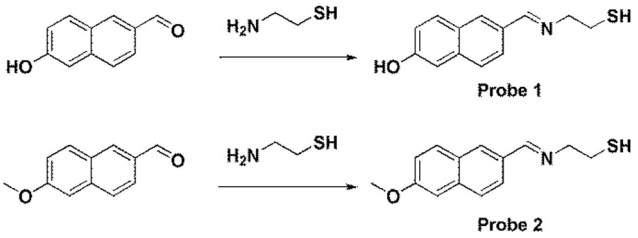

Scheme 1 Synthesis routes for **probe 1** and **probe 2**.

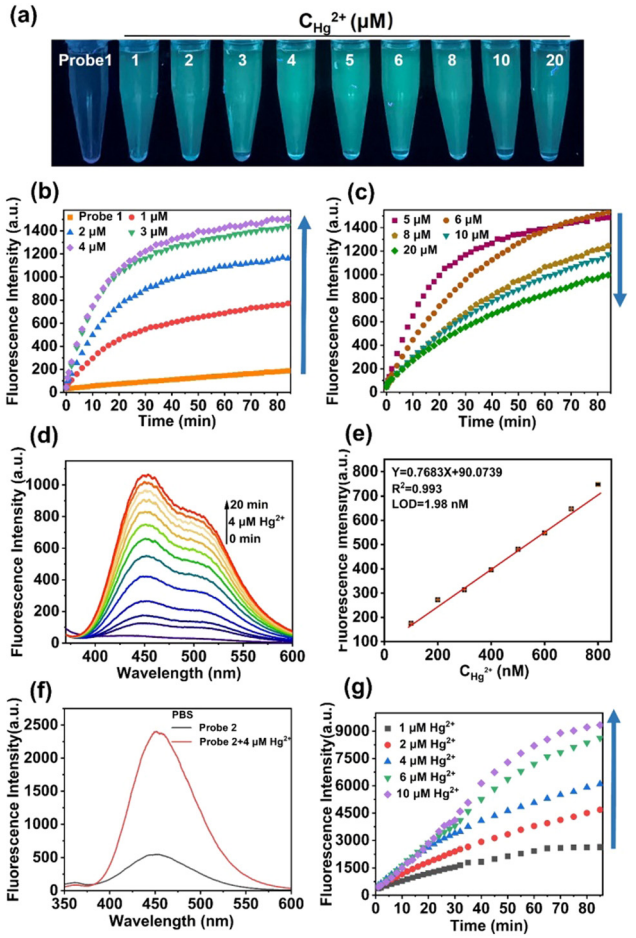

Fig. 1 Spectral studies of **probe 1** and **probe 2** with Hg^{2+}. (a) Fluorescence photographs of **probe 1** with different concentrations of Hg^{2+} under 365 nm UV light irradiation. (b) and (c) Time-dependent and concentration-dependent fluorescence spectra of **probe 1** (10 μM) in the presence of 1 μM, 2 μM, 3 μM, 4 μM, 5 μM, 6 μM, 8 μM, 10 μM, and 20 μM of Hg^{2+} in PBS buffer solution. (d) Time-dependent fluorescence spectra of **probe 1** (10 μM) in the presence of Hg^{2+} (4 μM) in PBS buffer solution. (e) The curve of F_{450} *versus* Hg^{2+} concentration in the range of 100 to 800 nM, indicating a good linear relationship. (f) The fluorescent response of **probe 2** (10 μM) with Hg^{2+} (4 μM) in PBS buffer solution. (g) Time-dependent and concentration-dependent fluorescence spectra of **probe 2** (10 μM) in the presence of 1 μM, 2 μM, 4 μM, 6 μM, and 10 μM of Hg^{2+} in PBS buffer solution.

After addition of Hg^{2+}, an obvious fluorescent enhancement was observed in PBS buffer solution because of the coordination of **probe 1** with Hg^{2+} that triggered the aggregation and excimer formation for fluorescence enhancement, and the ratio of fluorescence intensity in the presence and absence of Hg^{2+} was about 10.4-fold. The fluorescence intensity was nearly unchanged in other solutions (Fig. S7h, ESI†). In comparison, there was greater dispersion of coordination compounds in organic solvents, which prevented aggregation as compared to that in PBS buffer solution, and resulted in no fluorescence change. The detection procedures can also be conducted under different pH values, ranging from 5.8 to 8.0 (Fig. S8, ESI†).

The time-dependent and concentration-dependent fluorescence responses of **probe 1** in the presence of Hg^{2+} were determined (Fig. 1a–d). The fluorescence intensity dramatically increased upon addition of Hg^{2+} at the first 4 μM. Along with extended time (Fig. 1b), and then decreased with increasing concentrations from 5 μM to 20 μM (Fig. 1c). Moreover, visible colorimetric detection was applied under 365-nm excitation with the same tendency. The color changed from colorless to deep green as the concentration of Hg^{2+} increased from 1 μM to 4 μM, whereas it weakened to light green from 5 μM to 20 μM (Fig. 1a). The fluorescence intensity attained equilibrium as the time reached about 30 min (Fig. 1b). The detailed fluorescent spectral changes exhibited by **probe 1** with Hg^{2+} (4 μM) were also recorded (Fig. 1d). The fluorescence intensities at 450 nm exhibited a strong linear correlation with Hg^{2+} in the concentration range from 100 nM to 800 nM (Fig. 1e).

The limit of detection (LOD) was calculated to be 1.98 nM, which was greatly improved compared with the reported fluorescent probes in Table S1 (ESI†). The quantum yields of **probe 1** and **probe 1**-Hg^{2+} were calculated to be 4.1% and 8.2%, respectively (Fig. S9a, ESI†). The quantitative fluorescence lifetimes of **probe 1** and **probe 1**-Hg^{2+} were 1.6631 and 1.6698,

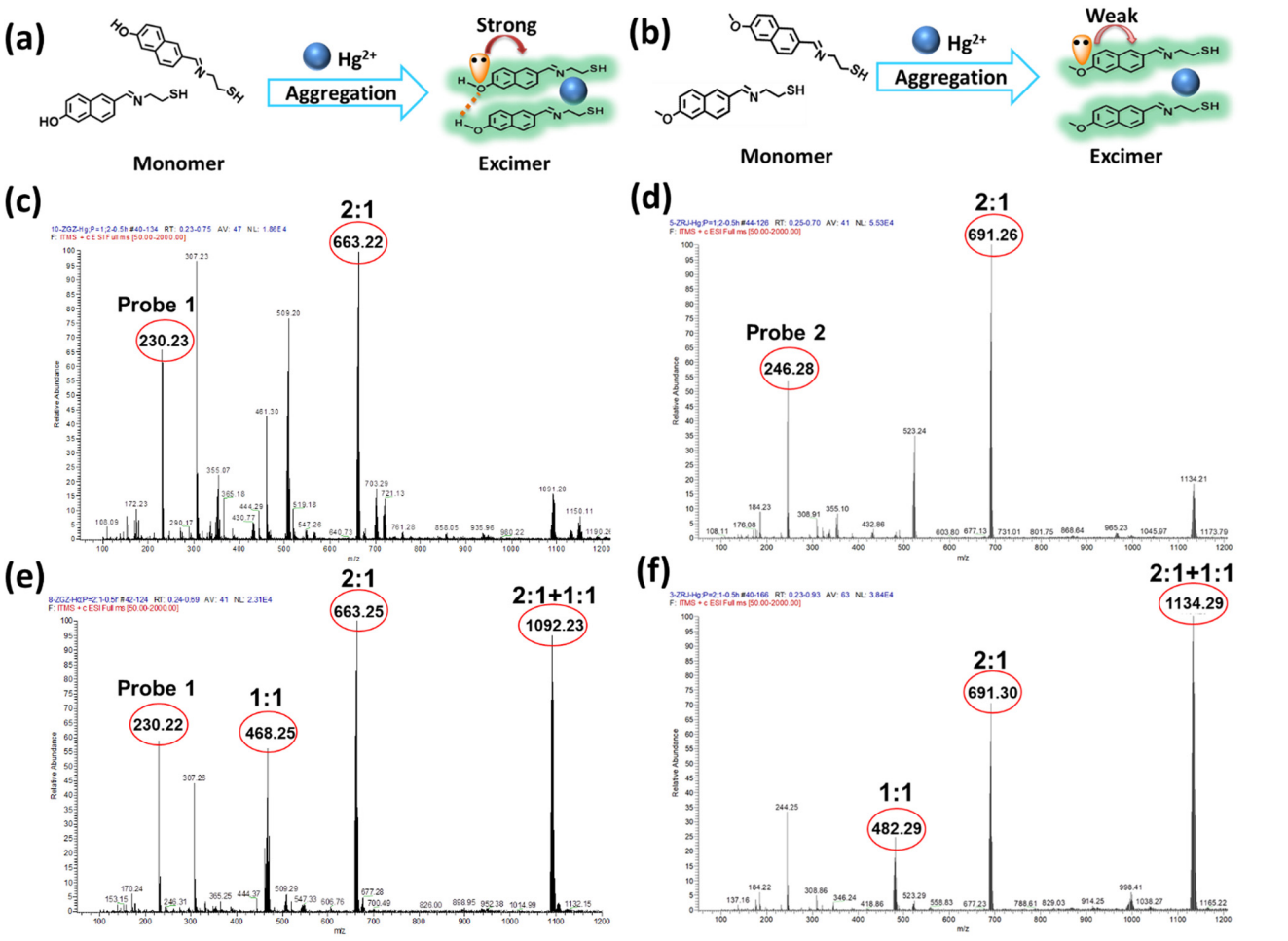

Fig. 2 The coordination mechanisms between probes 1 and 2 with Hg^{2+}. (a) and (b) Schematic diagrams of the excimer formation process of **probe 1** and **probe 2** with Hg^{2+}. (c) and (d) Mass spectra of the **probe 1**-Hg^{2+} (2 : 1) complex and **probe 2**-Hg^{2+} (2 : 1) complex. (e) Mass spectra of the **probe 1**-Hg^{2+} (1 : 2) complex (*m*/*z* 468.25 was assigned to a 1 : 1 complex, *m*/*z* 663.25 was assigned to a 2 : 1 complex, and *m*/*z* 1092.23 was assigned to a 2 : 1+1 : 1 complex). (f) The mass spectrum of the **probe 2**-Hg^{2+} (1 : 2) complex (*m*/*z* 482.29 was assigned to a 1 : 1 complex, *m*/*z* 691.30 was assigned to a 2 : 1 complex, and *m*/*z* 1134.29 was assigned to a 2 : 1+1 : 1 complex).

respectively (Fig. S10a and b, ESI†). UV-Vis spectra in the absence and presence of Hg^{2+} were also obtained using an absorption band at 320 nm increased over time (Fig. S11, ESI†).

The fluorescent changes of **probe 1** towards Hg^{2+} is a puzzling phenomenon and may be related to the reason for the high sensitivity of **probe 1** for ultra-low concentration detection of Hg^{2+}. To elucidate this phenomenon, contrast **probe 2** was synthesized for comparison. Parallel fluorescent and UV-Vis spectra experiments with **probe 2** were carried out, and Hg^{2+} detection was feasible in PBS solution (Fig. S12 and S13, ESI† and Fig. 1f). The time-dependent and concentration-dependent fluorescence responses of **probe 2** in the presence of Hg^{2+} were then determined.

As shown in Fig. 1g, the fluorescent intensity of **probe 2** in response to Hg^{2+} was enhanced as the concentration of Hg^{2+} increased and over extended time. The quantum yields of **probe 2** and **probe 2**-Hg^{2+} were calculated to be 10.9% and 17.6%, respectively (Fig. S9b, ESI†). The quantitative fluorescence lifetimes of **probe 2** and **probe 2**-Hg^{2+} were 5.3900 and 6.2103, respectively (Fig. S10c and d, ESI†). However, this was different from the fluorescent trends of **probe 1** (Fig. 1b and c).

Hence, mass spectroscopy was further performed to clarify the response mechanism. According to the spectral studies, the fluorescence intensity of **probe 1** and Hg^{2+} reached the maximum with a concentration ratio of 2 : 1 (Fig. 1b). Therefore, the electrospray ionization-mass spectrometry (ESI-MS) spectra of the probe-Hg^{2+} coordinated complexes with a ratio of 2 : 1 were measured. As shown in Fig. 2, the coordination mode of **probe 1** and **probe 2** with Hg^{2+} was confirmed to be 2 : 1, as suggested by their values of *m*/*z* 663.22 and 691.29, respectively (Fig. 2c and d).

In this case, the complexes of **probe 1**-Hg^{2+} and **probe 2**-Hg^{2+} mainly existed in a 2 : 1 ratio, and both of them were formed as excimer. However, when the probes and Hg^{2+} were mixed at the ratio of 1 : 2 (Fig. 2e and f), new peaks at 1092.23 and 1134.29 appeared for the **probe 1**-Hg^{2+} and **probe 2**-Hg^{2+} complexes, respectively. Different ratios of the probe-Hg^{2+} complexes were formed, and the excimer would be destroyed as the concentration of Hg^{2+} increased. **probe 1** and **probe 2** exhibited the same trends in the mass spectra of their complexes. All the results indicated that Hg^{2+} possessed the ability to trigger naphthalene-based fluorescent probes so they would form excimer and subsequently emit fluorescence, but this does not adequately explain the changes in fluorescence.

For structural analysis of the two probes, the only difference was in their different substituted groups—the hydroxyl group and methoxyl group. The Hammett substituent constants provide direct evidence of the higher electron-donating abilities of the hydroxyl group (−0.37) as compared to the methoxyl group (−0.27).[47] In **probe 1**, the lone pair of electrons in the hydroxyl group was intensively transferred to the naphthalene moiety, resulting in an augmented π-electron density that triggered the π–π electron stacking of the naphthalene conjugation and further facilitated the coordination of N and S atoms with Hg^{2+}. The enhancement of the fluorescence intensity was attributed to the formation of excimer with the extensive conjugated plane of naphthalene, as well as the rotation suppression of the C=N bond and the chelation enhanced fluorescence (CHEF) effect.

Density functional theory (DFT) studies were carried out to elucidate the possible mechanism. **probe 2** exhibited a higher energy gap between the HOMO–LUMO orbitals than **probe 1**, which was unfavorable for coordination with mercury ions due to its lower reactivity (Fig. S14a, ESI†). We also investigated the electron loss abilities of the naphthalene portion in two probes (Fig. S14b and Table S2, ESI†). The results (loss of 0.18442e in **probe 1** and loss of 0.18695e in **probe 2**) proved that the methoxyl group impeded the electron transfer to naphthalene, which is unfavorable for the formation of excimer. Besides, the lack of a hydrogen bond in the π–π stacking mode of **probe 2** directly weakened the stacking ability (Fig. S14c, ESI†). Therefore, the methoxyl group impeded the electron transfer to naphthalene and then weakened the π–π electron stacking, which is unfavorable for the formation of excimer. Moreover, the hydrogens in **probe 1** were shifted to a field that was higher than that of **probe 2** (Fig. S1 and S4, ESI†), which was derived from the stronger π–π stacking that increased the charge densities and further weakened the vibration of hydrogen. Based on these studies, it was determined that **probe 1** is more sensitive to low concentrations of Hg^{2+} in aqueous solutions, which is beneficial for bilateral fixation by hydrogen bond and mercury coordination to facilitate excimer formation as well as lone pair electrons to enhance the π–π electron stacking of the naphthalene conjugation.

To obtain insight into the fluorescent performance in a complicated matrix, selectivity studies were investigated in the presence of interfering metal ions (100 μM), including Cu^{2+}, Mg^{2+}, Fe^{3+}, Fe^{2+}, Cd^{2+}, K^{+}, Cr^{3+}, Ba^{2+}, Na^{+}, Mn^{2+}, Co^{2+}, Ca^{2+}, Ni^{2+}, Al^{3+}, Cu^{+}, Zn^{2+}, and Ag^{+}. As shown in Fig. 3, colorimetric detection under a 365-nm UV lamp was performed. **probe 1** (10 μM) was pre-introduced in PBS solution, and there

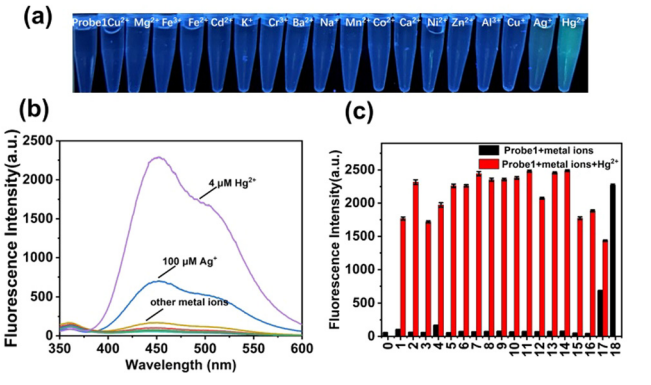

Fig. 3 (a) Fluorescence photograph of **probe 1** with different metal ions under 365-nm UV light irradiation. (b) Fluorescence spectra of **probe 1** with Hg^{2+} (4 μM) and other different metal ions (100 μM) in PBS buffer solution. (c) Relevant column diagram for selectivity studies of fluorescence **probe 1** with different metal ions (black bars, 0: **probe 1**, 1–18: Cu^{2+}, Mg^{2+}, Fe^{3+}, Fe^{2+}, Cd^{2+}, K^{+}, Cr^{3+}, Ba^{2+}, Na^{+}, Mn^{2+}, Co^{2+}, Ca^{2+}, Ni^{2+}, Zn^{2+}, Al^{3+}, Cu^{+}, Ag^{+}, and Hg^{2+}) and following the addition of Hg^{2+} (red bars) in PBS buffer solution (10 mM, pH 7.4). (λ_{ex} = 320 nm, λ_{em} = 450 nm).

were no obvious fluorescence color changes upon addition of these interfering metal ions except for Ag^{+} and Hg^{2+}. A slight green color and weak enhancement was exhibited after addition of Ag^{+}, as shown in (Fig. S15, ESI†), whereas a significant color transformation from colorless to deep green emerged upon addition of Hg^{2+}. The fluorescence intensities were further compared with each other, as shown in Fig. 3b and c, and only Hg^{2+} induced obvious emission enhancement (black bars), which increased to different extents in the presence of interfering metal ions (red bars). Therefore, **probe 1** exhibited high selectivity and sensitivity for the detection of Hg^{2+} in PBS buffer solution.

Determination of Hg^{2+} in real water samples

Having confirmed the excellent performances of the probes, **probe 1** was selected and then applied to evaluate the applicability of detection in real water samples, including tap water, ultrapure water, and lake water. As presented in Table 1, the determination of Hg^{2+} at ultra-low concentrations was conducted according to the standard addition method, and the recovery rates ranged from 91% to 108%. Therefore, **probe 1** can be effectively applied to measure Hg^{2+} in environmental water samples.

Imaging of Hg^{2+} in pea sprouts

As mentioned above, mercury can accumulate in the food chain, and plants are a key link because they act as repositories for mercury from the soil. Detection of Hg^{2+} in plants not only enables visualization of mercury distribution and bioaccumulation in plants, but also facilitates the use of effective methods to avoid mercury damage. Hence, pea sprouts were employed as a plant model for fluorescent imaging. Four-day-old pea sprouts were incubated with **probe 1** for 12 hours, and then incubated with mercury for another 12 hours. The longitudinal and transverse root sections were then imaged under a 10x objective lens. Fig. 4 shows that the fluorescent emissions were quite weak when the tissues were only incubated with **probe 1**. Once Hg^{2+} was added, it was transferred into the plant tissues through plant veins and exhibited bright fluorescent emission. The results indicate that **probe 1** was capable of visualization imaging of mercury in plants.

Table 1 Determination of Hg^{2+} in real water samples

Sample	Added (nM)	Found (nM) and RSD (n = 3)	Recovery (%)
Tap water	0	Not detected	—
	200	215.58 ± 0.97	108
	500	540.29 ± 0.23	108
	800	810.27 ± 0.40	101
Ultrapure water	0	Not detected	—
	200	210.27 ± 1.36	105
	500	464.81 ± 0.31	93
	800	744.51 ± 0.06	93
Lake water	0	Not detected	—
	200	181.20 ± 0.29	91
	500	507.00 ± 0.61	101
	800	791.92 ± 0.29	99

Experimental

Materials and instruments

All chemical reagents were analytical grade and purchased from commercial sources, and were used without further purification. Fluorescent probes were characterized by NMR and ESI-MS spectra using a Bruker AVANCE IIITM 500 spectrometer and a Thermo LCQ Fleet mass spectrometer, respectively. Fluorescent spectral studies were recorded on a fluorescence spectrophotometer (HITACHI F-4700). The mechanisms of probe coordination with Hg^{2+} were confirmed by mass spectra. Fluorescence imaging of slices of pea sprouts was obtained using an Olympus fluorescent microscope (FluoView FV1000). DFT calculations were carried out by the Gaussian 16 program packages. All structures were fully optimized at the M06-2X+GD3/def2-TZVP level. Natural atomic charges were generated using the NBO 6.0 program.

Spectral analysis

The spectral analysis was conducted in phosphate-buffered saline (PBS, 10 mM, pH 7.4). The stock solutions of probes (10 mM and 1 mM) were prepared using analytically pure dimethyl sulfoxide (DMSO) and stored at 4 °C, and then diluted to a working concentration (10 μM, 0.1% DMSO) with PBS buffer solution. Deionized water was used to prepare 10 mM individual stock solutions of Cu^{2+}, Mg^{2+}, Fe^{3+}, Fe^{2+}, Cd^{2+}, K^{+}, Cr^{3+}, Ba^{2+}, Na^{+}, Mn^{2+}, Co^{2+}, Ca^{2+}, Ni^{2+}, Al^{3+}, Cu^{+}, Zn^{2+}, Ag^{+}, and Hg^{2+}. Selective and competitive experiments of **probe 1** (10 μM) in the presence of Hg^{2+} (4 μM) and with potential interference (100 μM) were conducted in PBS buffer solution after 60 minutes. The lake water, tap water, and ultrapure water were mixed with PBS buffer solution (1 : 19, v/v) and then assessed with working concentrations of **probe 1** (10 μM) and Hg^{2+} (0 to 800 nM).

Preparation of the slices of pea sprouts

Pea seeds were sterilized with ethanol and cultured in ultrapure water medium at room temperature. Roots of four-day-old pea sprouts were incubated with **probe 1** (10 μM) for 12 hours and Hg^{2+} (20 μM) for 12 hours in cascade. After thoroughly washing with ultrapure water, the roots (mature zone) were embedded in 4% low melting point agarose. Longitudinal and transverse cutting was implemented using a vibrating microtome (VT1200S, Leica), and the roots were cut into semi-thin sections of 100-μm thickness. The sections were placed on microscope slides, infiltrated with PBS, and then covered with a coverslip. Fluorescence imaging for slices of pea sprouts in longitudinal and transverse cutting forms was performed, and the sprouts were observed under an Olympus fluorescence microscope with a 10× objective lens. The excitation wavelength was at 405 nm, and the collecting wavelengths were from 400 to 500 nm.

Synthesis of probe 1

In a 50-mL round-bottomed flask, 6-hydroxy-2-naphthaldehyde (172 mg, 1 mmol) and mercaptoethylamine (77 mg, 1 mmol) were dissolved in 5 mL anhydrous ethanol under stirring, and then refluxed for 30 min. The reaction progress was monitored

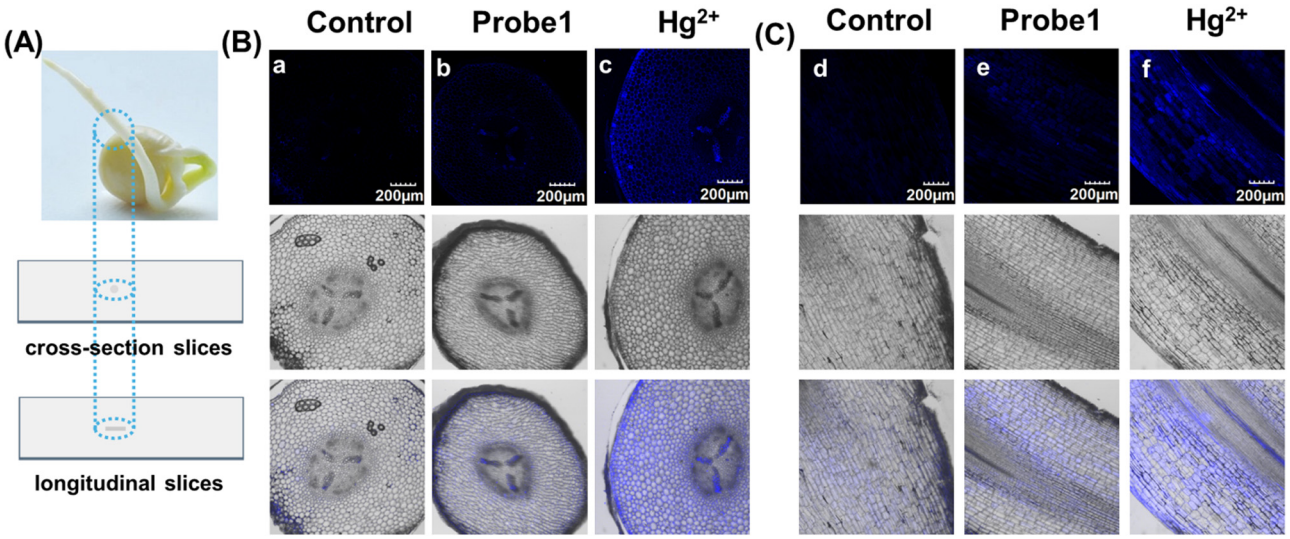

Fig. 4 Fluorescence imaging of **probe 1** for Hg^{2+} determination in pea sprouts. (A) Photograph of a pea sprout and schematic diagrams of root slices. (B) Fluorescence imaging of cross-section slices of pea sprouts. (a) Blank group. (b) Slices of pea sprouts incubated with **probe 1** (10 μM) for 12 h. (c) Slices of pea sprouts incubated with **probe 1** (10 μM) for 12 h and then treated with Hg^{2+} (20 μM) for 12 h. (C) Fluorescence imaging of longitudinal slices of pea sprouts. (d) Blank group. (e) Slices of pea sprouts incubated with **probe 1** (10 μM) for 12 h. (f) Slices of pea sprouts incubated with **probe 1** (10 μM) for 12 h and then treated with Hg^{2+} (20 μM) for 12 h. Scale bars = 200 μm (λ_{ex} = 405 nm, λ_{em} = 400–500 nm).

by thin-layer chromatography (TLC). At the end of the reaction, the crude product was filtered to obtain a white solid (**probe 1**) with a yield of 58%. ^{1}H NMR (500 MHz, DMSO-d_6) δ 9.75 (s, 1H), 7.81 (s, 1H), 7.72 (d, J = 8.7 Hz, 1H), 7.65 (d, J = 8.6 Hz, 1H), 7.47 (dd, J = 8.6, 1.6 Hz, 1H), 7.16–6.99 (m, 2H), 5.58 (s, 1H), 3.52 (ddd, J = 11.4, 5.1, 3.4 Hz, 1H), 3.08–2.81 (m, 3H). ^{13}C NMR (126 MHz, DMSO-d_6) δ 155.48, 134.86, 134.13, 129.35, 127.19, 126.13, 125.77, 125.41, 118.84, 108.61, 73.43, 52.88, 36.31. ESI-MS $[C_{13}H_{13}NOS]^+$, calcd. 231.07, found $[M+1]^+$: 232.19.

Synthesis of probe 2

In a 50-mL round-bottomed flask, 6-methoxy-2-naphthaldehyde (186 mg, 1 mmol) and mercaptoethylamine (116 mg, 1.5 mmol) were dissolved in 5 mL anhydrous ethanol under stirring, and then refluxed for 30 min. The reaction was monitored by TLC. At the end of the reaction, the crude product was filtered to obtain a white solid (**probe 2**) with a yield of 60%. ^{1}H NMR (500 MHz, DMSO-d_6) δ 7.88 (s, 1H), 7.83–7.73 (m, 2H), 7.54 (dd, J = 8.5, 1.7 Hz, 1H), 7.30 (d, J = 2.4 Hz, 1H), 7.16 (dd, J = 8.9, 2.6 Hz, 1H), 5.61 (s, 1H), 3.87 (s, 3H), 3.57–3.44 (m, 1H), 3.11–2.85 (m, 3H). ^{13}C NMR (126 MHz, DMSO-d_6) δ 157.37, 135.94, 133.81, 129.31, 127.99, 126.78, 126.04, 125.34, 118.78, 105.84, 73.28, 55.19, 52.87, 36.34. ESI-MS $[C_{14}H_{15}NOS]^+$, calcd. 245.34, found $[M+1]^+$: 246.22.

Conclusions

In summary, we successfully constructed naphthalene-based fluorescent **probe 1** for detection of ultra-low concentrations of mercury. We synthesized contrast **probe 2** to use fluorescence and mass spectra to deeply study the response mechanism, which can be ascribed to three key factors. First, the sulfhydryl and C=N group of the Schiff base were responsible for the coordination between probes and Hg^{2+}, which was conducive to inducing excimer formation and then subsequent turn-on fluorescence emission. Second, the hydroxyl group of **probe 1** formed an intermolecular hydrogen bond, but this could not occur in **probe 2**. The bilateral fixation by hydrogen bond and coordination further enhanced the stability of the excimer. Third, the key factor for fluorescence enhancement of **probe 1** was speed, because the lone pair of electrons of the hydroxyl group could easily transfer to the naphthalene moiety, resulting in an augmented π-electron density that further enhanced the π–π electron stacking. For these reasons, **probe 1** is more sensitive to low concentrations of Hg^{2+} in aqueous solutions, with a calculated detection limit of 1.98 nM. Hence, **probe 1** was successfully applied to detect Hg^{2+} in water samples and pea sprouts. This holds significant importance for the determination of mercury contamination and bioaccumulation, with potential application for contamination warning in advance.

Author contributions

Shujing Fang: investigation, writing – original draft. K. M. K. Swamy: investigation. Wen-Yan Zan: writing – review and editing. Juyoung Yoon: conceptualization, writing – review and editing. Shudi Liu: conceptualization, writing – original draft, writing – review and editing.

Data availability

The data supporting this article have been included as part of the ESI.†

Conflicts of interest

There are no conflicts to declare.

Acknowledgements

This work was financially supported by the Natural Science Foundation of China (21701074). J. Yoon thanks the National Research Foundation (NRF) funded by the Korean government (MSIT) (2022R1A2C3005420 and 2020R1A6C101B194). K. M. K. Swamy thanks the Brain Pool program funded by the Ministry of Science and ICT through the National Research Foundation of Korea (RS-2023-00304224).

Notes and references

1 B. Gao, L. Han, H. Hao and H. Zhou, *Ecol. Indic.*, 2016, **67**, 577–585.
2 K. G. Pavithra, P. SundarRajan, P. S. Kumar and G. Rangasamy, *Chemosphere*, 2023, **312**, 137314.
3 T. W. Clarkson, L. Magos and G. J. Myers, *N. Engl. J. Med.*, 2003, **349**, 1731–1737.
4 T. W. Clarkson, *Crit. Rev. Clin. Lab. Sci.*, 2008, **34**, 369–403.
5 T. W. Clarkson and L. Magos, *Crit. Rev. Toxicol.*, 2006, **36**, 609–662.
6 S. Liu, X. Zhang, C. Yan, P. Zhou, L. Zhang, Q. Li, R. Zhang, L. Chen and L. Zhang, *J. Hazard. Mater.*, 2022, **424**, 127701.
7 Y. Wang, L. Zhang, X. Han, L. Zhang, X. Wang and L. Chen, *Chem. Eng. J.*, 2021, **406**, 127166.
8 T. A. Saleh, G. Fadillah, E. Ciptawati and M. Khaled, *TrAC, Trends Anal. Chem.*, 2020, **132**, 116016.
9 J. Yin, L. Huang, L. Wu, J. Li, T. D. James and W. Lin, *Chem. Soc. Rev.*, 2021, **50**, 12098–12150.
10 X. Qian and Z. Xu, *Chem. Soc. Rev.*, 2015, **44**, 4487–4493.
11 J. Du, M. Hu, J. Fan and X. Peng, *Chem. Soc. Rev.*, 2012, **41**, 4511–4535.
12 S. Liu, L. Zhang, H. Kim, J. Sun and J. Yoon, *Coord. Chem. Rev.*, 2024, **501**, 215575.
13 D. Rajput, N. Pradhan, S. Mansuri, V. Soppina and S. Kanvah, *J. Mater. Chem. B*, 2024, **12**, 4698–4707.
14 Z. L. Li, A. X. Ma, J. Q. Liu, K. Wang, B. C. Zhu, D. W. Pang and D. M. Kong, *J. Mater. Chem. B*, 2024, **12**, 4398–4408.
15 R. AbhijnaKrishna and S. Velmathi, *Coord. Chem. Rev.*, 2022, **459**, 214401.
16 H. Shuai, C. Xiang, L. Qian, F. Bin, L. Xiaohui, D. Jipeng, Z. Chang, L. Jiahui and Z. Wenbin, *Dyes Pigm.*, 2021, **187**, 109125.
17 S.-Y. Chen, Z. Li, K. Li and X.-Q. Yu, *Coord. Chem. Rev.*, 2021, **429**, 213691.
18 S. Liu, D. Feng, L. Zhang, H. Song, Y. Wang, X. Zhang, Q. Zhao and L. Chen, *Spectrochim. Acta, A*, 2020, **243**, 118817.
19 E. M. Nolan and S. J. Lippard, *Chem. Rev.*, 2008, **108**, 3443–3480.
20 A. Kumar, Virender, M. Saini, B. Mohan, Shayoraj and M. Kamboj, *Microchem. J.*, 2022, **181**, 107798.
21 S. Fang, L. Zhang, Y. Zhao, X. Zhang, L. Zhang, L. Chen, J. Yoon and S. Liu, *Sens. Actuators, B*, 2024, **411**, 135768.
22 A. K. Jha, S. Umar, R. K. Arya, D. Datta and A. Goel, *J. Mater. Chem. B*, 2016, **4**, 4934–4940.
23 A. S. Belova, Y. N. Kononevich, D. S. Ionov, V. A. Sazhnikov, A. D. Volodin, A. A. Korlyukov, P. V. Dorovatovskii, M. V. Alfimov and A. M. Muzafarov, *Dyes Pigm.*, 2023, **208**, 110852.
24 C. Wang, X. Yang, R. Duan, X. Li, Y. Liu, W. Liu, B.-G. He, S. Zhang, B. Yang, K. Wang, B. Zou, Y. Qi, Q. Li, H. Liu and Y. Dai, *Dyes Pigm.*, 2024, **223**, 111953.
25 Y. Chen, *Molecules*, 2022, **27**, 8628.
26 Y. Chen, S. Zheng, M. H. Kim, X. Chen and J. Yoon, *Curr. Opin. Chem. Biol.*, 2023, **75**, 102321.
27 S. Zeng, X. Liu, Y. S. Kafuti, H. Kim, J. Wang, X. Peng, H. Li and J. Yoon, *Chem. Soc. Rev.*, 2023, **52**, 5607–5651.
28 R. Long, C. Tang, Q. Wei, C. Tong, X. Tong, S. Shi, Y. Guo and Y. Yang, *Sens. Actuators, B*, 2021, **348**, 130666.
29 J.-B. Li, Y. Liu, X.-J. Zheng and D. Wang, *Microchem. J.*, 2019, **150**, 104123.
30 S. Chatterjee, H. Gohil, I. Raval, S. Chatterjee and A. R. Paital, *Small*, 2019, **15**, e1804749.
31 Z. Xu, J. Yoon and D. R. Spring, *Chem. Commun.*, 2010, **46**, 2563–2565.
32 J. Cui, H. Nie, X. Liang, J. Bai and X. Zhang, *J. Mol. Liq.*, 2022, **366**, 120325.
33 G. Han, D. Kim, Y. Park, J. Bouffard and Y. Kim, *Angew. Chem.*, 2015, **54**, 3912–3916.
34 Y. Wang, J. Chen, Y. Chen, W. Li and C. Yu, *Anal. Chem.*, 2014, **86**, 4371–4378.
35 S. Bhuin, P. Sharma, P. Chakraborty, O. P. Kulkarni and M. Chakravarty, *J. Mater. Chem. B*, 2023, **11**, 188–203.
36 X. Chen, K. H. Baek, Y. Kim, S. J. Kim, I. Shin and J. Yoon, *Tetrahedron*, 2010, **66**, 4016–4021.
37 K. Inoue, R. Kawakami, M. Murakami, T. Nakayama, S. Yamamoto, K. Inoue, T. Tsuda, K. Sayama, T. Imamura, D. Kaneno, S. Hadano, S. Watanabe and Y. Niko, *J. Mater. Chem. B*, 2022, **10**, 1641–1649.
38 X. Gou, M. A. H. Nawaz, C. Liu, N. Yang, J. Ren, H. Zhou, Y. Li, J. Zhu, W. Han and C. Yu, *J. Mater. Chem. B*, 2022, **10**, 5774–5783.
39 L. Wang, C. Lou, M. Zhao, B. Zhao, H. Zhao, W. Ma, A. Wang, X. Wang, N. Wang and Y. Li, *Inorg. Chem. Commun.*, 2021, **129**, 108662.
40 T. Puangsamlee, Y. Tachapermpon, P. Kammalun, K. Sukrat, C. Wainiphithapong, J. Sirirak and N. Wanichacheva, *J. Lumin.*, 2018, **196**, 227–235.
41 X. J. Wang, G. W. Li, Y. P. Cheng, Q. L. Sun, Y. Q. Hao, C. H. Wang and L. T. Liu, *Front. Chem.*, 2022, **10**, 813108.
42 Y. Gao, H. Liu, S. Zhang, Q. Gu, Y. Shen, Y. Ge and B. Yang, *Phys. Chem. Chem. Phys.*, 2018, **20**, 12129–12137.
43 X. Wu, N. Duan, S. Yang, H. Tian and B. Sun, *ChemistrySelect*, 2020, **5**, 1683–1687.
44 X. Wu, N. Duan, Y. Li, S. Yang, H. Tian and B. Sun, *J. Photochem. Photobiol., A*, 2020, **388**, 112209.
45 B. Musikavanhu, Y. Liang, Z. Xue, L. Feng and L. Zhao, *Molecules*, 2023, **28**, 6960.
46 N. Kumari, S. Singh, M. Baral and B. K. Kanungo, *J. Fluoresc.*, 2023, **33**, 859–893.
47 C. Hansch, A. Leo and R. W. Taft, *Chem. Rev.*, 2002, **91**, 165–195.

